Supporting Information

Fong et al. 10.1073/pnas.1008291107

Materials and Methods.

Human Corneal Epithelial (HCE) Cell Culture. Primary human corneal epithelial cells were obtained from ScienCell Research Laboratories and Cascade Biologics. All cells were maintained in serum-free EpiLife culture medium (with 60 μM $CaCl_2$, Cascade Biologics) supplemented with Human Corneal Growth Supplement (HCGS containing bovine pituitary extract, bovine insulin, hydrocortisone, bovine transferrin, and mouse epidermal growth factor, Cascade Biologics). Gentamicin (10 μg/ml) and amphotericin (0.25 μg/ml) were also added to culture media. Serum-free EpiLife medium was used in all experiments to exclude extracellular matrix proteins (i.e., fibronectin, laminin) present in serum. Cells in passages 2 to 7 were used.

Cell Spreading. Aliquots (500 μl) of FN and BSA solutions were added to the wells of a transparent 24-well plate (Falcon BD, VWR) and allowed to adsorb overnight at 4 ºC. In these experiments, fibronectin (FN, 10 μg/ml in PBS, Chemicon) was used as a positive control and bovine serum albumin (BSA, 2 mg/ml in PBS, Sigma) was used as a negative control. Subsequently, wells were rinsed twice with prewarmed PBS solution and blocked with 500 μl of 0.2 wt% heat-inactivated BSA solution at room temperature for 30 min. At the same time, coverslips containing spin-coated aECM protein films were mounted in empty wells by dotting sterile grease around the circumference of the coverslips. Gentle pressure was applied to ensure firm adhesion to the well. Finally, all wells were rinsed twice with prewarmed PBS solution.

HCE cells were enzymatically passaged using 0.05% Trypsin-0.25% EDTA (Cascade Biologics). To each well, 4.8×10^4 cells were added together with 1 ml of fresh EpiLife medium. The plates were swirled gently to prevent clustering of cells and placed in an incubator at 37 ºC under 5% CO_2/95% air. Images of five random positions in each well were acquired after 4 h. Using ImageJ, 200 cells were traced for each surface and their areas were recorded. Cells with projected areas above 300 μm^2 (based on the average cell areas on BSA), cells were considered spread and the percentage of spread cells was plotted for each surface.

Characterization of Cross-Linked aECM Films by Atomic Force Microscopy (AFM). Images and force curves were collected on an Asylum MFP-3D-BIO atomic force microscope, with accompanying IGOR Pro v.5.05 software. Pyramidal-tipped silicon nitride cantilevers (Veeco DNP-S) with nominal spring constant 0.58 N/m were used for imaging. The tip of a pair of fine forceps was drawn lightly across the surface of the protein film, prepared as described above, tearing away the protein along the scratch and exposing the underlying glass substrate. The edge of the scratch was imaged by AFM both dry and in water, and the thickness of the film was determined. Scans were made at various positions along the scratch to obtain an average measurement. The average film thickness was calculated by averaging the height measurements obtained from 5 positions, using the revealed glass as a baseline. Thicknesses measured on three separate films were averaged.

For nanoindentation studies, tips with 600 nm SiO_2 microspheres attached at the tip end (Novascan Technologies) were used (1). Protein films with predetermined thicknesses were immersed in water for at least 1 h at room temperature to allow equilibrium water uptake. Both the films and the cantilever assembly were submerged in water under ambient conditions during nanoindentation. Force curves were collected; the instrument records z (piezo) displacement and force, the product of measured tip deflection and cantilever spring constant. The maximum indentation force was set to 50 nN relative to the contact point. The tip speed was 1 μm/ sec, and data were collected at 0.5 Hz.

The spring constants of the tips used for nanoindentation were determined to be about 0.3 N/m using thermal calibration in water. The Dimitriadis model (2) for indentation of linear-elastic soft material films of finite height with a spherical indenter was applied to the loading force data. Only force-indentation points between 20 nm and 10% maximum indentation were used to constrain the data to the near-linear response range. The elastic modulus was obtained by averaging the calculated moduli at multiple points in three separate films.

Dehydrated films were determined to be in the range of 193 ± 19 nm ($n = 70$) in thickness; hydrated films were 349 ± 26 nm ($n = 36$) thick. Based on measured height differences, water content in hydrated films was estimated to be approximately 45%. The elastic modulus of a hydrated film was determined to be 0.24 ± 0.06 MPa ($n = 21$), which falls within the range previously determined for films of similar aECM proteins (1). There were no discernible physical differences among films with varying RGD concentrations.

A typical surface used for studying the crossing probabilities was imaged by AFM (Fig. S2). The height of the step at the boundary was 119 ± 14 nm ($n = 30$).

Estimation of RGD Surface Density. The surface density of RGD domains in each film was estimated by assuming a density of elastin of 1.32 g/cm^3, a protein weight fraction of 0.45 (determined by comparing wet and dry films by AFM), and an accessible surface depth of 10 nm.

Extracting Simulation Parameters from Single Cell Spreading Data. As explained in *Materials and Methods* (Eq. **9**), the connection between the spreading and retraction rates on surfaces with the same RGD fraction, φ_{RGD}, is

$$\tilde{W}_r(\varphi_{RGD}) = \exp(f'\gamma'/k_BT)[A - \tilde{W}_s(\varphi_{RGD})] - k\exp(-\varepsilon_{el}/k_BT)/W_s(FN) \quad \textbf{[S1]}$$

where $A \equiv k\exp(-\varepsilon_{el}/k_BT + f\gamma/k_BT)/W_s(FN)$. If we assume that the binding energy, ε is proportional to the RGD fraction on the surface, i.e., $\varepsilon = \tilde{\varepsilon}\varphi_{RGD}$, we get

$$\tilde{W}_s = A - B\exp(-\tilde{\varepsilon}\varphi_{RGD}/k_BT) \quad \textbf{[S2]}$$

where $B \equiv k/W_s(FN)$.

The percent spread cells on aECM with different RGD concentrations after 4 h (shown in Fig. 1*E*) relative to the percent of spread cells on FN after 4 h, was taken as a measure for the relative rate of cell spreading, $\tilde{W}_s$ and was fitted to Eq. **S2**. Out of the fit we obtain $A = 1.11$. The fit is shown in Fig. S3.

Derivation of an Expression for the Proliferation Rate. The number of cells confined to a single lattice site is denoted by n_1 (red circle, Fig. S4); the number of spread on two adjacent lattice sites by n_2 (red oval, Fig. S4). The empty square in Fig. S4 represents an empty neighboring site on the lattice. The rates for spreading, retraction and proliferation steps are denoted by W_s, W_r, and W_p, respectively.

In our model, only cells that are spread on two adjacent lattice sites can proliferate. This assumption is consistent with the observation that decreased cell spreading can inhibit proliferation signals (3), and it creates an effective time lag between consecutive cell divisions, resembling interphase (4).

The rate equations for the kinetic scheme illustrated in Fig. S4 are

$$\frac{dn_1}{dt} = -W_s n_1(1 - n_1/n_1^* - n_2/n_2^*) + W_r n_2 + 2W_p n_2 \qquad \textbf{[S3]}$$

$$\frac{dn_2}{dt} = W_s n_1(1 - n_1/n_1^* - n_2/n_2^*) - W_r n_2 - W_p n_2. \qquad \textbf{[S4]}$$

The first term is the rate of spreading, where the probability to find a neighboring empty lattice site is taken to be the mean field probability, i.e., $P_{\text{empty}_{\text{site}}} = (1-\theta)$ where θ is the fraction of occupied sites on the lattice and is given by $\theta = n_1/n_1^* + n_2/n_2^*$ where n_1^* is the number of cells that occupy a single site when at confluence. Likewise, n_2^* is the number of cells that occupy two adjacent sites at confluence.

The change in the total number of cells $n = n_1 + n_2$ is then

$$\frac{dn}{dt} = \frac{dn_1}{dt} + \frac{dn_2}{dt} = W_p n_2. \qquad \textbf{[S5]}$$

Since for most cases, $W_p \ll W_r$, W_s, we can assume fast equilibrium in order to solve the rate equations (Eqs. **S3** and **S4**). In the limit of low cell concentration ($n_1/n_1^* \ll 1$), we get the expected exponential growth

$$\frac{dn}{dt} = \frac{W_p}{1 + (\frac{W_r}{W_s})} n. \qquad \textbf{[S6]}$$

The doubling time, t_D, for a cell population which grows according to the kinetic scheme presented in Fig. S4 is

$$t_D = \frac{\ln 2}{W_p}(1 + W_r/W_s). \qquad \textbf{[S7]}$$

According to the literature, the doubling time for human corneal epithelial (HCE) cells is estimated to be 25 h (5). Using the values for W_r and W_s on FN, we get $W_p = 0.05\ \text{h}^{-1}$. We assume that W_p is identical on all the surfaces. We find that this treatment overestimates the contribution of proliferation to wound healing, but that the calculated variation in proliferation rates from surface to surface is modest, as observed experimentally (Fig. S7 *B* and *C*).

Including Cell–Cell Interactions in the Simulation. Wound-healing behavior depends not only on cell-aECM interaction but also on intercellular interaction. The energy of a cell fluctuates, but unlike in a fluid, the origin of the fluctuations is not collisions with the solvent or the thermal energy. The fluctuations in energy in a cellular system originate from fluctuations around the steady state of the biochemical networks of the cell (6). Consequently, it is accepted to define an effective temperature $T_{\text{eff}} = F_T/k_B$ where F_T is the magnitude of the energy fluctuations and k_B is the Boltzmann constant (7–9). As a result, the probability of a cell to have an energy fluctuation ε' is $\exp(-\varepsilon'/F_T)$.

In the simulation, we measure the intercellular interaction energy between nearest neighbor cells, $\varepsilon_{\text{cell-cell}}$, in units of F_T. The interaction energy between cells comes into play in the simulation for the case of cell retraction. When a cell retracts, there is an active force that pulls it from the surface and from its neighbors as explained in the model for spreading and retraction (see *Materials and Methods*). This force can either lead to cell–cell bond breakage or to retraction of the cell, pulling the neighboring cell along.

Let us denote the number of neighbors that the cell in question would lose upon retraction by υ. The cell can retract and break the bonds with its neighbors with a probability $W_r \times (\exp(-\varepsilon_{\text{cell-cell}}/F_T))^{\upsilon}$. Alternatively, the cell can retract, break the bonds with $\upsilon - 1$ of its neighbors and pull the remaining cell with it with probability $W_r \times (\exp(-\varepsilon_{\text{cell-cell}}/F_T))^{\upsilon-1}$. A neighboring cell can only be stretched if it occupies a single lattice site. This is to ensure that the total elastic energy of the cell does not exceed the cell fluctuation energy F_T.

HCE cells are characterized by relatively weak cell–cell contacts and behave much like a weakly interacting liquid. We quantified the dynamic behavior of the cell sheet by measuring experimentally the average cell–cell bond survival time. The average bond survival time was 1.64 ± 0.24 hours. Fig. S5 shows the dependence of the average bond survival time in the simulation on the interaction energy. The interaction energy value that best mimics the behavior observed experimentally is $\varepsilon_{\text{cell-cell}}/F_T = 0.7$.

Single Cell Crossing Rates. When a cell is at the boundary, it can either cross the boundary with a rate constant, k_c or move away from the boundary with a rate constant, k_b as illustrated in the schematic in Fig. S6*A*.

From the time-lapse movies, we recorded the time spent by the cell at the boundary until a reaction occurs (i.e., waiting time), as well as the outcome (i.e., crossing or moving away). In order to extract the rate constant for boundary crossing from the experiment, it is necessary to know the waiting time distribution for cells at the boundary.

Let us define $P_0(t;t_0)$ as the probability that no event occurs in the interval $(t_0, t_0 + t)$ and assume that the events are independent and the rate constants do not depend on time. Then, $P_0(t + dt; t_0) = P_0(t;t_0) \times (1 - \sum_i k_i dt)$, where k_i is the rate constant for event i (in our case: $i = c,b$).

Consequently, $\frac{P_0(t+dt;t_0) - P_0(t;t_0)}{dt} = (-\sum_i k_i) P_0(t;t_0)$.

And in the limit of $dt \to 0$, we get: $\frac{dP_0(t)}{dt} = (-\sum_i k_i) P_0(t)$ so that $P_0(t) = \exp(-\sum_i k_i \times t)$.

We denote the waiting time distribution as $w(t)$. The waiting time distribution can be expressed as $w(t) = (P_0(t) - P_0(t + dt))/dt = -dP_0(t)/dt$ and hence,

$$w(t) = K \exp(-Kt) \qquad \textbf{[S8]}$$

where $K = \sum_i k_i$ is the sum of the rate constants for all possible events.

Using the waiting time distribution (Eq. **S8**), the average waiting time is

$$\langle t \rangle = \frac{\int_0^\infty t \times K \exp(-Kt) dt}{\int_0^\infty K \exp(-Kt) dt} = \frac{1}{K}. \qquad \textbf{[S9]}$$

In the case of the cell crossing experiment, the waiting at the boundary can end with either crossing of the boundary (k_c) or with moving away from the boundary (k_b). Thus, the average waiting time becomes: $\langle t \rangle = 1/(k_c + k_b)$.

If we define N_c as the number of events which end with boundary crossing and N as the total number of events, we get

$$\frac{N_c}{N} = \frac{k_c}{k_c + k_b}. \qquad \textbf{[10]}$$

Using Eqs. **S8–S10**, the rate constant of boundary-crossing can be expressed as

$$k_c = \frac{N_c}{N\langle t \rangle}. \qquad \textbf{[S11]}$$

Notice that according to Eq. **S11**, the rate constant of boundary crossing, k_c, can be calculated as the number of crossing events divided by the total waiting time at the boundary, $t_{\text{total}} = N\langle t \rangle$.

1. Nowatzki PJ, Tirrell DA (2003) Physical properties of artificial extracellular matrix protein films prepared by isocyanate crosslinking. *Biomaterials* (25):1261–1267.
2. Dimitriadis EK, Horkay F, Maresca J, Kachar B, Chadwick RS (2002) Determination of elastic moduli of thin layers of soft materials using the atomic force microscope. *Biophys J* 82:2798–2810.
3. Nelson CM, Chen CS (2002) Cell-cell signaling by direct contact increases cell proliferation via a PI3K-dependent signal. *FEBS Lett* 514:238–242.
4. Alberts B et al. (2008) *Molecular Biology of the Cell* (Garland Science, New York) pp 637–655.
5. Kahn CR, Young E, Lee IH, Rhim JS (1993) Human corneal epithelial primary cultures and cell-lines with extended life-span—in-vitro model for ocular studies. *Invest Opthalmol Vis Sci* 34:3429–3441.
6. Goodwin BC (1963) *Temporal Organization in Cells: A Dynamic Theory of Cellular Control Processes* (Academic Press, New York) pp 55–80.
7. Beysens DA, Forgacs G, Glazier JA (2000) Cell sorting is analogous to phase ordering in fluids. *Proc Natl Acad Sci USA* 97:9467–9471.
8. Neagu A, Jakab K, Jamison R, Forgacs G (2005) Role of physical mechanisms in biological self-organization. *Phys Rev Lett* 95:178101–178104.
9. Drasdo D, Hohme S (2005) A single-cell-based model of tumor growth in vitro: Monolayers and spheroids. *Phys Biol* 2:133–147.

aECM-RGD:

M-MASMTGGQQMG-HHHHHHH-DDDDK(LD-YAVTG**RGD**SPASSKIA((VPGIG)$_2$VPG*K*G(VPGIG)$_2$)$_4$VP)$_3$-LE

T7 tag; His tag; Cleavage site; RGD cell-binding domain; Elastin-like domain

aECM-RDG:

M-MASMTGGQQMG-HHHHHHH-DDDDK(LD-YAVTG**RDG**SPASSKIA((VPGIG)$_2$VPG*K*G(VPGIG)$_2$)$_4$VP)$_3$-LE

Scrambled RGD cell-binding domain

Fig. S1. Amino acid sequences of aECM proteins containing RGD and RDG cell-binding domains. Each aECM protein contained a T7 tag, a hexahistidine tag, an enterokinase cleavage site, and elastin-like domains containing lysine residues (italicized) for cross-linking.

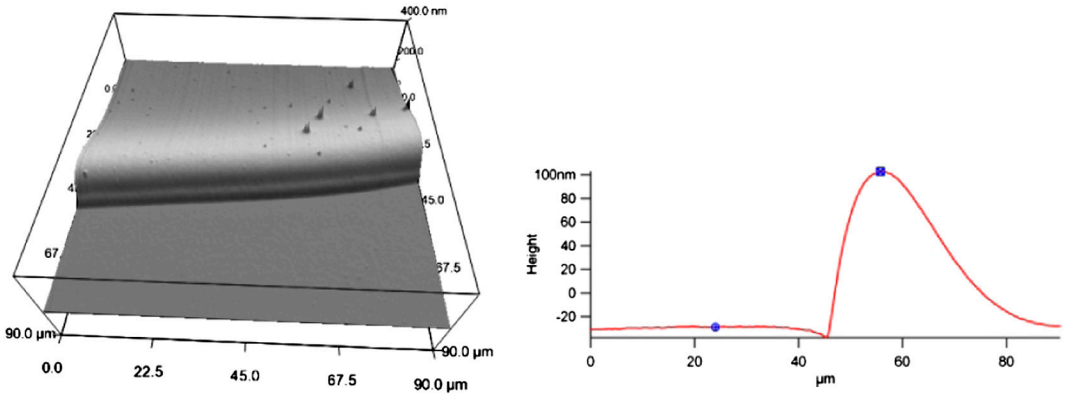

Fig. S2. Image of typical substrate with a boundary imaged by atomic force microscopy (left). A cross-section of the boundary region is also shown (right).

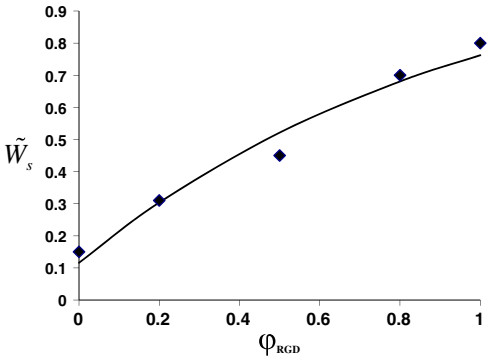

Fig. S3. The fit of the experimental spreading data to the theoretical expression for the relative spreading rate, Eq. **S2**.

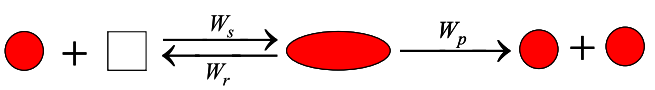

Fig. S4. An illustration of the proliferation kinetic scheme. The white box represents an empty neighboring lattice site on which the cell can spread in order to proliferate.

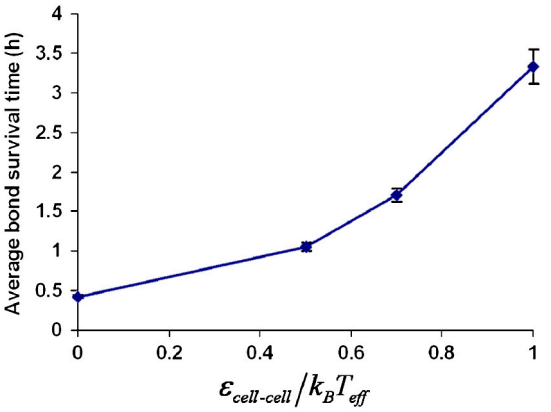

Fig. S5. The average bond survival time as a function of the cell–cell interaction energy in the simulation.

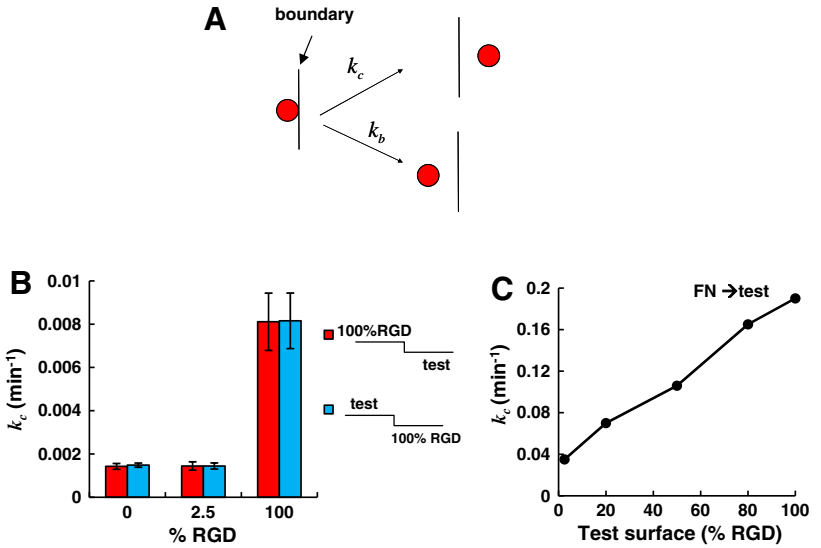

Fig. S6. (*A*) Schematic diagram of cell at a boundary, showing two possible outcomes. A cell can cross the boundary with a rate constant k_c, or it can move away with a rate constant, k_b. (*B*) Rate constants of boundary crossing, k_c, from 100% RGD into various test surfaces. The crossing probabilities computed for both configurations of the boundary. There were no significant differences between the rate constants for the two configurations of each test surface, suggesting that the small "step" at the boundary did not affect the boundary-crossing rate. (*C*) Rate constants of boundary crossing from FN to test surfaces obtained from simulation. The crossing rates from 100% RGD to 100% RGD and from 100% RGD to 2.5% RGD differ by a factor of five, consistent with experimental observations (Table S1).

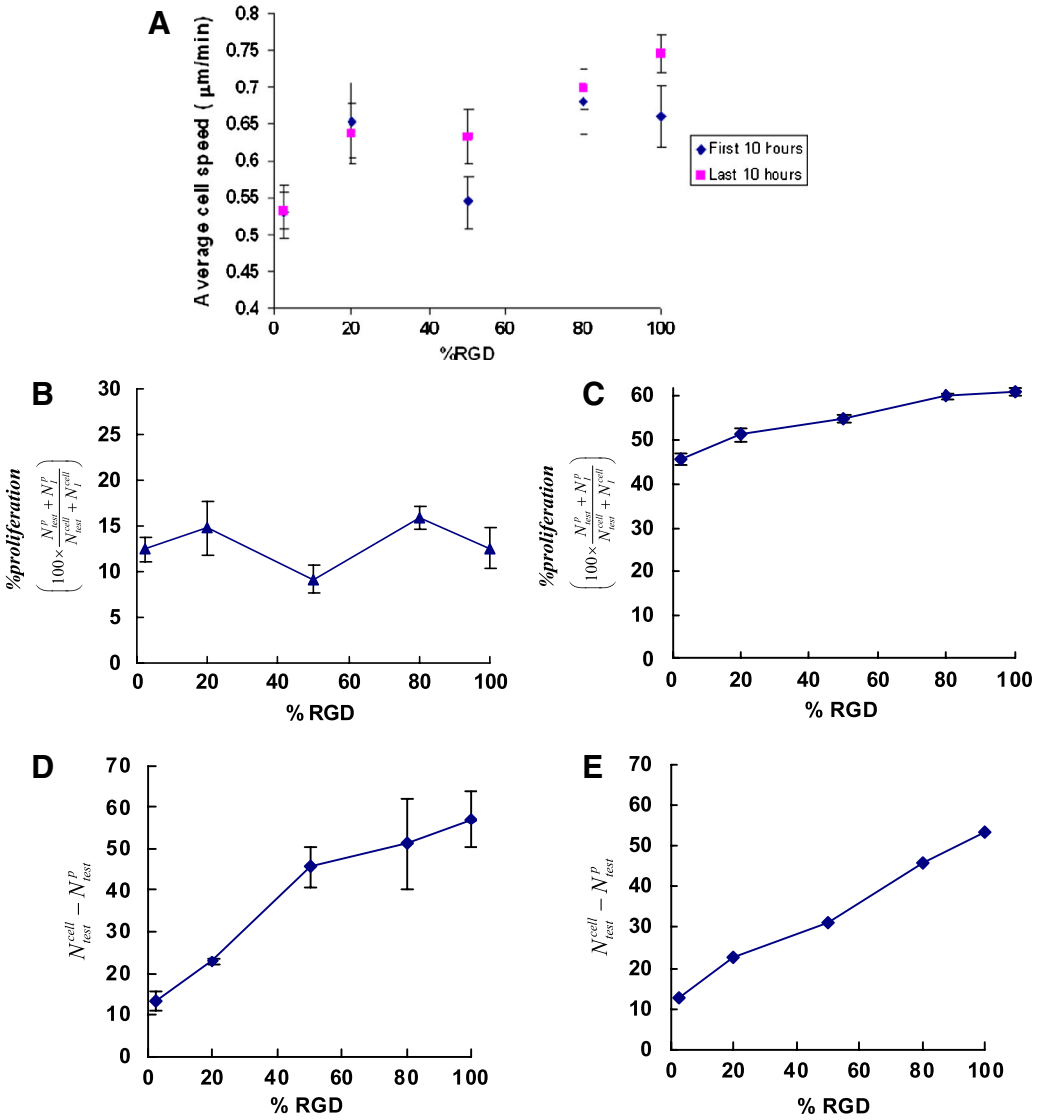

Fig. S7. Contributions to wound closure. (*A*) Comparison of average cell speeds for the first and last 10-h periods after wounding. (*B*) Proliferation on the test surface and in the interfacial region in the experiment. (*C*) Proliferation on the test surface and in the interfacial region in the simulation. (*D*) Numbers of cells in the wound area at $t = 30$ h that crossed the boundary during the experiment. (*E*) Numbers of cells in the wound area at $t = 30$ h that crossed the boundary in the simulation. Numbers are reported in (*D*) and (*E*) for a boundary length equal to 15 cell diameters. See Table S2 for definitions of symbols and raw data.

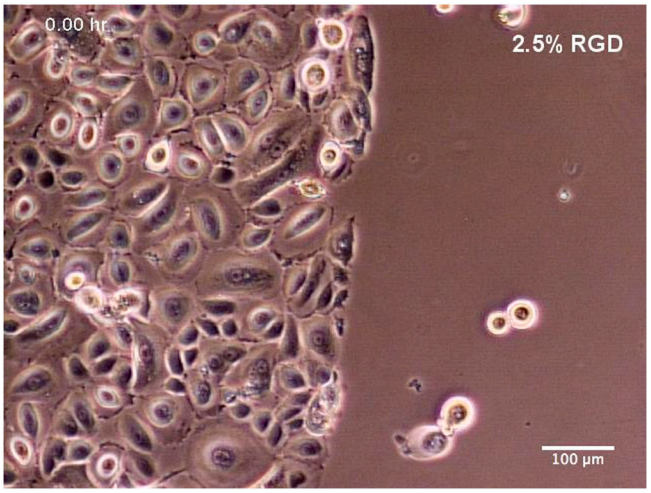

Movie S1. Epithelial wound healing on 2.5% RGD.

Movie S1 (AVI)

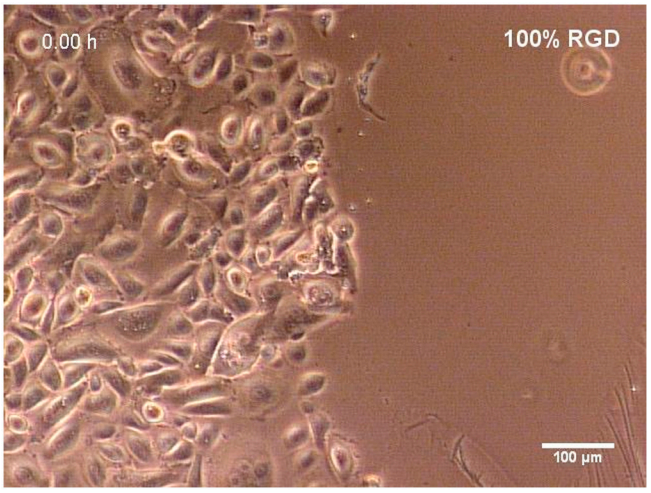

Movie S2. Epithelial wound healing on 100% RGD.

Movie S2 (AVI)

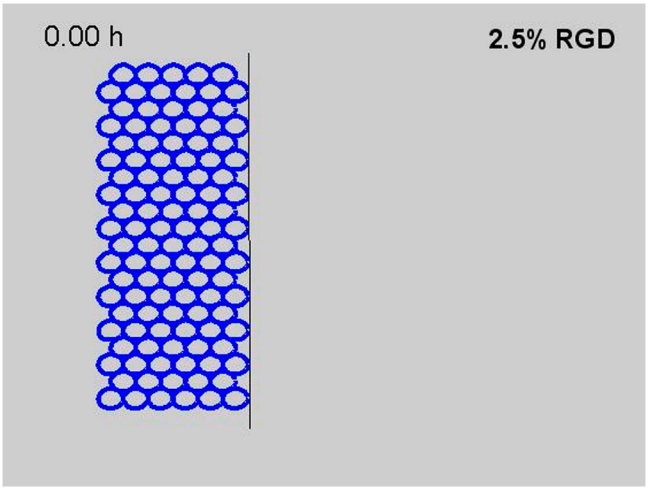

Movie S3. Simulation of wound healing on 2.5% RGD.

Movie S3 (AVI)

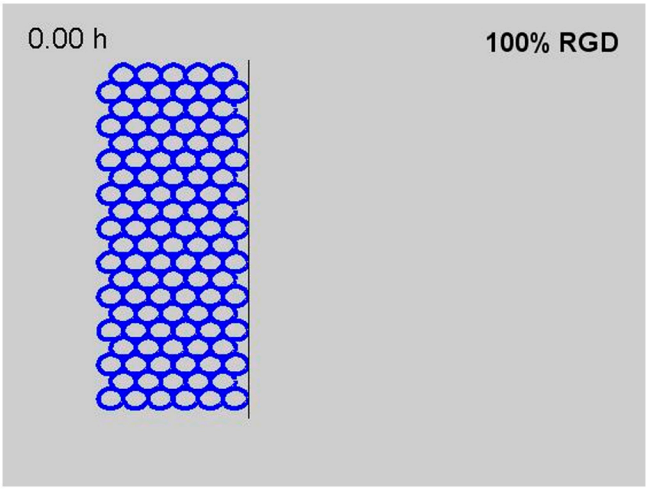

Movie S4. Simulation of wound healing on 100% RGD.

Movie S4 (AVI)

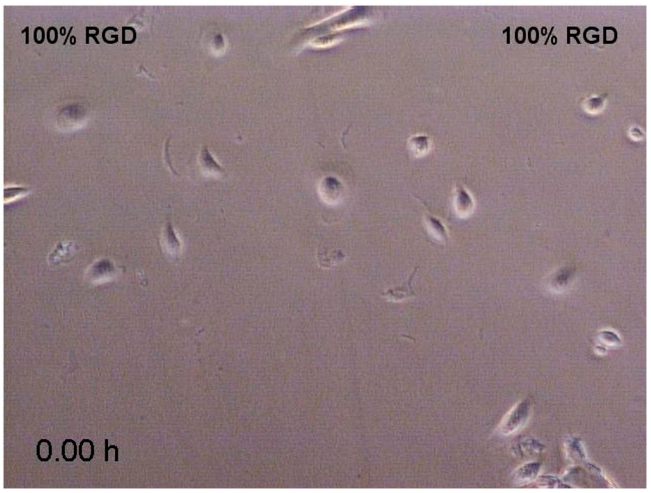

Movie S5. Single cell boundary crossing from 100% RGD to 100% RGD.
Movie S5 (AVI)

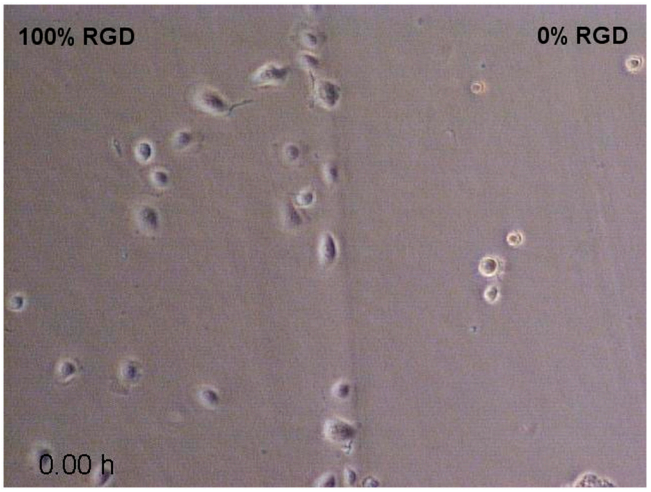

Movie S6. Single cell boundary crossing from 100% RGD to 0% RGD.
Movie S6 (AVI)

Table S1. Summary of the rates for 100% and 2.5% RGD surfaces

	Simulation	Experiment
Surface composition (the line represents the wound edge at time $t = 0$)	FN|RGD	FN|RGD
Wound-closure rate (μm/h) (100% RGD)	9.4	9.6
Wound-closure rate (μm/h) (2.5% RGD)	1.7	1.7
Wound-closure rate ratio (100% RGD/2.5% RGD)	5.6	5.6
Single cell speed ratio (100% RGD/2.5% RGD)	1.9	1.4

Table S2. Experimental numbers of cells and proliferation events on the test surface and in the interfacial region

	Sample #	N_{test}^{cell}	N_{test}^{p}	$N_{test}^{cell} - N_{test}^{p}$	$\frac{N_{test}^{p}}{N_{test}^{cell}}$	N_{I}^{cell}	N_{I}^{p}	$\frac{N_{I}^{p}}{N_{I}^{cell}}$	$\frac{(N_{test}^{p}+N_{I}^{p})}{(N_{test}^{cell}+N_{I}^{cell})}$
100% RGD	1	34	1	33	0.029	31	4	0.129	0.077
	2	51	3	48	0.059	30	0	0.000	0.037
	3	65	5	60	0.077	27	5	0.185	0.109
	4	60	7	53	0.117	42	8	0.190	0.147
	5	46	5	41	0.109	32	1	0.031	0.077
	6	52	4	48	0.077	33	5	0.152	0.106
	7	72	16	56	0.222	30	11	0.367	0.265
	8	71	18	53	0.254	35	13	0.371	0.292
	9	34	1	33	0.029	13	0	0.000	0.021
	10	59	8	51	0.136	29	4	0.138	0.136
	11	120	22	98	0.183	26	5	0.192	0.185
	12	120	7	113	0.058	36	5	0.139	0.077
100% RGD	Mean	65.33	8.08	57.3	0.112	30.33	5.08	0.158	0.127
	SEM	7.84	1.9	6.7	0.020	1.923	1.11	0.033	0.023
80% RGD	1	20	4	16	0.200	18	4	0.222	0.211
	2	20	1	19	0.050	20	5	0.250	0.150
	3	28	4	24	0.143	13	0	0.000	0.098
	4	98	15	83	0.153	18	4	0.222	0.164
	5	68	10	58	0.147	17	2	0.118	0.141
	6	101	16	85	0.158	23	3	0.130	0.153
	7	90	16	74	0.178	35	8	0.229	0.192
80% RGD	Mean	60.7	9.43	51.3	0.147	20.57	3.714	0.167	0.158
	SEM	13.02	2.25	10.8	0.017	2.46	0.874	0.031	0.0127
50% RGD	1	31	2	29	0.065	32	2	0.063	0.063
	2	46	6	40	0.130	23	4	0.174	0.145
	3	50	4	46	0.080	23	0	0.000	0.055
	4	60	7	53	0.117	17	2	0.118	0.117
	5	64	4	60	0.063	24	3	0.125	0.080
50% RGD	Mean	50.2	4.6	45.6	0.09082	23.8	2.2	0.0958	0.092
	SEM	5.19	0.78	4.77	0.012	2.14	0.593	0.0266	0.015
20% RGD	1	32	9	23	0.281	41	13	0.317	0.301
	2	28	3	25	0.107	23	2	0.087	0.098
	3	26	3	23	0.115	25	3	0.120	0.118
	4	24	2	22	0.083	23	3	0.130	0.106
	5	24	5	19	0.208	31	3	0.097	0.145
	6	28	3	25	0.107	24	3	0.125	0.115
20% RGD	Mean	27	4.17	22.8	0.150	27.833	4.5	0.146	0.147
	SEM	1.13	0.96	0.83	0.029	2.65	1.56	0.032	0.029
2.5% RGD	1	9	0	9	0.000	23	4	0.174	0.125
	2	30	4	26	0.133	40	11	0.275	0.214
	3	12	0	12	0.000	21	3	0.143	0.091
	4	5	0	5	0.000	21	2	0.095	0.077
	5	15	2	13	0.133	25	3	0.120	0.125
	6	8	0	8	0.000	31	4	0.129	0.103
	7	23	2	21	0.087	20	3	0.150	0.116
	8	13	1	12	0.077	36	6	0.167	0.143
2.5% RGD	Mean	14.34	1.13	13.3	0.054	27.13	4.5	0.157	0.124
	SEM	2.75	0.48	2.3	0.02	2.52	0.95	0.018	0.014

The interfacial region is defined as a region one spread-cell diameter (130 μm) deep next to the interface on the cell-sheet side (outside the wound). N_{test}^{cell} and N_{I}^{cell} denote the numbers of cells on the test surface and in the interfacial region, respectively, after 30 h. N_{test}^{p} and N_{I}^{p} denote the numbers of proliferation events on the test surface and in the interfacial region, respectively, during a 30-h period. Each sample corresponds to analysis of a separate movie of a wound-healing experiment.